Am J Physiol Heart Circ Physiol 320: H1774–H1785, 2021.
First published March 5, 2021; doi:10.1152/ajpheart.00877.2020

american physiological society

AMERICAN JOURNAL OF PHYSIOLOGY
HEART AND CIRCULATORY PHYSIOLOGY

RESEARCH ARTICLE

Exercise and Cardiac Remodeling in Normal and Athletic States

Geometrical remodeling of the mitral and tricuspid annuli in response to exercise training: a 3-D echocardiographic study in elite athletes

Alexandra Fábián,[1]* Bálint Károly Lakatos,[1]* Márton Tokodi,[1] Anna Réka Kiss,[1] Nóra Sydó,[1,2] Emese Csulak,[1] Erika Kispál,[1] Máté Babity,[1] Andrea Szűcs,[1] Orsolya Kiss,[1,2] Béla Merkely,[1,2]* and Attila Kovács[1]*

[1]*Semmelweis University Heart and Vascular Center, Budapest, Hungary and* [2]*Department of Sports Medicine, Semmelweis University, Budapest, Hungary*

Abstract

Intense exercise exposes the heart to significant hemodynamic demands, resulting in adaptive changes in cardiac morphology and function. Nevertheless, the athletic adaptation of the atrioventricular valves remains to be elucidated. Our study aimed to characterize the geometry of mitral (MA) and tricuspid (TA) annuli in elite athletes using 3-D echocardiography. Thirty-four athletes presented with functional mitral regurgitation (FMR) were retrospectively identified and compared with 34 athletes without mitral regurgitation (MR) and 34 healthy, sedentary volunteers. 3-D echocardiographic datasets were used to quantify MA and TA geometry and leaflet tenting by dedicated softwares. MA and TA areas, as well as tenting volumes, were higher in athletes compared with controls. MA area was significantly higher in athletes with MR compared with those without (8.2 ± 1.0 vs. 7.2 ± 1.0 cm^2/m^2, $P < 0.05$). Interestingly, athletes with MR also presented with a significantly higher TA area (7.2 ± 1.1 vs. 6.5 ± 1.1 cm^2/m^2, $P < 0.05$). Nonplanar angle describing the MA's saddle shape was less obtuse in athletes without MR, whereas the values of athletes with MR were comparable with controls. The exercise-induced relative increases in left ventricular (35 ± 25%) and left atrial (40 ± 29%) volumes were similar; however, the increment in the MA area was disproportionately higher (63 ± 23%, overall $P < 0.001$). The relative increase in TA area (40 ± 23%) was also higher compared with the increment in right ventricular volume (34 ± 25%, $P < 0.05$). Atrioventricular annuli undergo a disproportionate remodeling in response to regular exercise. Athletic adaptation is characterized by both annular enlargement and increased leaflet tenting of both valves. There are differences in MA geometry in athletes presented with versus without FMR.

NEW & NOTEWORTHY We have characterized the annular geometry of mitral and tricuspid valves in elite athletes using 3-D echocardiography. We have found that exercise-induced remodeling of the atrioventricular annuli comprises a disproportionate dilation of annular dimensions and increased leaflet tenting of both valves. Moreover, we have demonstrated a more pronounced saddle shape of the mitral annulus in athletes without mitral regurgitation, which was not present in those who had mild regurgitation.

3-D echocardiography; athlete's heart; functional mitral regurgitation; mitral annulus; tricuspid annulus

INTRODUCTION

Regular, intense physical exercise results in complex adaptive changes in the morphology and function of the heart (1). Nevertheless, the vast majority of data are related to the ventricles and the atria (2). A balanced dilation of the cardiac chambers is a characteristic and unequivocal feature of an athlete's heart. Although ventricular and atrial dilation can significantly affect atrioventricular annular geometry and related valvular competency in various pathological states, less is known about the exercise-induced alterations in the shape and function of the mitral and tricuspid annuli in elite athletes (3).

Primary valvular heart diseases show the same prevalence in athletes than in the general population (4). However, mitral and tricuspid insufficiency is reported more frequently among athletes, suggesting predominantly secondary (functional) origin (5). The classical ventricular type of functional regurgitation is mainly characterized by increased leaflet tenting, whereas a notably enlarged annulus rather refers to atrial functional regurgitation (3). The athlete's heart shares several features of both types of functional regurgitation: pronounced ventricular and atrial dilation may even exaggerate their impact on annular geometry and valvular function. Thus, a mixed type of functional regurgitation can be assumed in athletes presented with mitral or tricuspid insufficiency.

* A. Fábián, A. Kovács, B. K. Lakatos, and B. Merkely contributed equally to this work.
Correspondence: A. Kovács (attila.kovacs@med.semmelweis-univ.hu).
Submitted 29 October 2020 / Revised 29 January 2021 / Accepted 26 February 2021

Our current study aimed to characterize the geometry of mitral and tricuspid annuli in elite athletes compared with healthy, sedentary volunteers using three-dimensional (3-D) echocardiography. We hypothesized that atrioventricular annuli undergo a disproportionate remodeling in contrast to cardiac chambers, and there is a difference in the mitral annular geometry between athletes presented with versus without mitral regurgitation.

METHODS

As part of our Center's complex sports cardiology screening program, we retrospectively identified healthy athletes with 3-D transthoracic echocardiographic datasets available for detailed analysis of the left and right hearts. Using this cohort, we have selected those athletes who presented with at least mild mitral regurgitation (MR). Exclusion criteria were *1*) presence of any primary cause for MR revealed at the first report or during the review process of the previously acquired datasets (including prolapse, billowing, cleft, etc.), *2*) suboptimal 3-D dataset image quality for the analysis of the annuli, and *3*) noncompatible image source, as tricuspid annular (TA) quantification is available only by a single vendor. An additional age-matched cohort of athletes was selected from our database with the same sex distribution but no mitral regurgitation. An age-matched healthy, sedentary population (<3 h of exercise/wk) with the same sex distribution served as the control group having neither MR nor tricuspid regurgitation (TR). Detailed medical history and training regime were obtained along with a standard physical examination and 12-lead ECG. Two-dimensional (2-D) and 3-D echocardiography and then cardiopulmonary exercise testing (CPET) were performed on all athletes on the same day. All participants provided written, informed consent to study procedures. Our study is in accordance with the Declaration of Helsinki and approved by the Medical Research Council (ETT-TUKEB No. 13687-0/2011-EKU).

Cardiopulmonary Exercise Testing

CPET for peak oxygen uptake ($\dot{V}O_2$ and $\dot{V}O_2$/kg) quantification was performed on a treadmill until the exhaustion of the athletes. The volume and composition of the expired gases were analyzed breath by breath using an automated cardiopulmonary exercise system (Respiratory Ergostik, Geratherm, Bad Kissingen, Germany). Subjects were encouraged to achieve maximal effort, which was confirmed by respiratory exchange ratio, by lactate curves by regular fingertip lactate measurements every 2 min during the test, and by reaching the predicted maximal heart rate and a plateau in $\dot{V}O_2$.

2-D and 3-D Echocardiography

Transthoracic echocardiographic examinations were performed on a commercially available ultrasound system (E95, 4Vc-D probe, GE Vingmed Ultrasound, Horten, Norway). A standard acquisition protocol consisting of 2-D loops from parasternal, apical, and subxiphoid views was applied. Beyond conventional echocardiographic examination, ECG-gated full-volume 3-D datasets reconstructed from four cardiac cycles optimized for the left or the right heart were obtained for further analysis on a separate workstation (Fig. 1). Left ventricular (LV) internal diameters and wall thicknesses; left atrial (LA) 2-D end-systolic volume; mitral inflow velocities and *E* wave deceleration time; systolic (s'), early diastolic (e'), and atrial (a') velocities of the mitral lateral and septal annulus; average E/e'; right ventricular (RV) basal short-axis diameter, tricuspid annular plane systolic excursion (TAPSE), fractional area change (FAC), and TA velocities; and right atrial (RA) 2-D end-systolic volume were measured according to current guidelines (6).

MR was graded based on the measurement of vena contracta width (VCW), preferably on zoomed color parasternal long-axis view loops at the narrowest portion of the regurgitation jet as it emerges beyond the orifice. Mild MR was defined as having a measurable vena contracta but with a width of <0.3 cm as per current guidelines (7). "Non-MR" was defined as an absolutely not or just barely detectable jet, no flow convergence, and not having measurable vena contracta with a faint, incomplete, or no continuous-wave Doppler signal. Similarly, TR grading was based on measuring the VCW. TR jet was established either on apical four-chamber or in parasternal right ventricular (RV) inflow views. Mild TR was defined as a small jet but with measurable VCW (<0.3 cm). Lack of TR was defined as an absolutely not or just barely detectable jet, no flow convergence, and not having measurable VCW with a faint, incomplete, or no continuous-wave Doppler signal.

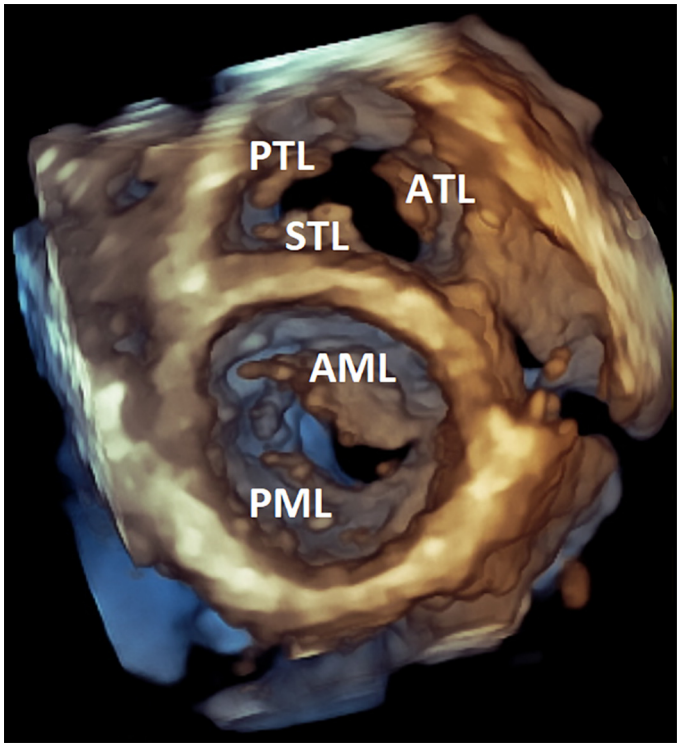

Figure 1. Representative volume-rendered three-dimensional (3-D) transthoracic echocardiographic image of an athlete's heart (diastolic frame). Using an apical perspective, anterior mitral valve leaflet (AML), posterior mitral valve leaflet (PML), septal tricuspid valve leaflet (STL), posterior tricuspid valve leaflet (PTL), and anterior tricuspid valve leaflet (ATL) are visible. The generally excellent transthoracic windows of athletes represented the basis for our advanced mitral and tricuspid valve measurements.

3-D datasets focused on the left heart were processed using semiautomated, commercially available softwares (4D LV-Analysis 3, TomTec Imaging, Unterschleissheim, Germany, and EchoPAC v204, 4D Auto LAQ, GE). We determined LV end-diastolic volume index (EDVi), end-systolic volume index (ESVi), stroke volume index (SVi), and LV mass index (LV Mi). To assess global LV function, ejection fraction (EF), global longitudinal strain (GLS), and global circumferential strain (GCS) were also calculated. Concerning the 3-D quantification of the LA, we measured maximal (LAV_{max}) and minimal (LAV_{min}) volumes and the volume at the onset of atrial contraction (LAV_{preA}). Using these volumetric data, we calculated LA total emptying fraction as $100 \times (LAV_{max} - LAV_{min})/LAV_{max}$, LA passive emptying fraction as $100 \times (LAV_{max} - LAV_{preA})/LAV_{max}$, and LA active emptying fraction as $100 \times (LAV_{preA} - LAV_{min})/LAV_{preA}$, as parameters of LA reservoir, conduit, and contractile function, respectively. The analysis of the 3-D datasets focused on the right heart was performed using 4D RV-Function 2 software (TomTec Imaging). We quantified 3-D RV EDVi, ESVi, and SVi, EF, and septal and free wall two-dimensional (2-D) longitudinal strain as well. Concerning the 3-D quantification of the RA, we used the same software as for the LA (EchoPAC v204, 4D Auto LAQ, GE) due to the lack of dedicated RA software package. Similarly, we measured maximal (RAV_{max}) and minimal (RAV_{min}) volumes and the volume at the onset of atrial contraction (RAV_{preA}). Using these volumetric data, we calculated RA total emptying fraction as $100 \times (RAV_{max} - RAV_{min})/RAV_{max}$, RA passive emptying fraction as $100 \times (RAV_{max} - RAV_{preA})/RAV_{max}$, and RA active emptying fraction as $100 \times (RAV_{preA} - RAV_{min})/RAV_{preA}$, as parameters of RA reservoir, conduit, and contractile function, respectively.

3-D Quantification of Mitral and Tricuspid Annuli

Mitral annulus (MA) was quantified by a commercially available software (EchoPAC v204, 4D Auto MVQ, GE) previously validated against other mitral valve quantification softwares and also against transesophageal image acquisition and subsequent analysis (8). First, the automatic selection of end-diastolic and end-systolic time points was confirmed by visual assessment of cardiac cycle events. Then, the orientation of the 3-D dataset was aligned to conform with prespecified standard views. A midsystolic reference frame was automatically selected, which was subsequently used to report static parameters. Six anatomical landmark points were placed using the two standard orthogonal planes (commissural and long-axis views), and then, the software created the 3-D model of the mitral valve annulus and leaflets. If needed, model contours could be modified manually throughout the cardiac cycle. Reported MA and leaflet parameters are as follows (also presented graphically on Fig. 2): 3-D MA area, 2-D MA area (projected 2-D area at the level of the best-fit plane), MA perimeter, MA anteroposterior diameter, MA posteromedial-anterolateral diameter, commissural diameter, intertrigonal distance, MA sphericity index (the ratio between anteroposterior and posteromedial-anterolateral diameters), MA height, MA nonplanar angle (describing the MA saddle shape), annulus height to commissural width ratio (ACHWR, describing the MA saddle shape), MA systolic excursion, MA maximal systolic velocity, MA area fraction, mitral-aortic angle, anterior and posterior leaflet lengths, areas, angles, tenting height, area, and volume.

TA was quantified by commercially available software (EchoPAC v204, 4-D Auto TVQ, GE). First, the automatic selection of end-diastolic and end-systolic time points was confirmed by visual assessment of cardiac cycle events. Then, the orientation of the 3-D dataset was aligned by the placement of tricuspid valve center point and adjusting RV long-axis to conform with prespecified standard views. A midsystolic reference frame was automatically selected, which was subsequently used to report static parameters. Five anatomical landmark points were placed using the two standard orthogonal planes (4-chamber and RV 2-chamber views), and then, the software created the 3-D model of the tricuspid valve annulus and leaflets. If needed, model contours could be modified manually throughout the cardiac cycle. Reported TA and leaflet parameters are as follows (also presented graphically on Fig. 3): 3-D TA area, 2-D TA area (projected 2-D area at the level of the best-fit plane), TA area fraction, TA perimeter, TA diameter on four-chamber view, TA diameter on two-chamber view, TA major and minor axes, sphericity index (the ratio between four-chamber view and two-chamber view diameters), TA systolic excursion, maximal tenting height, and tenting volume.

Parameters were normalized to body surface area (BSA) calculated by the Mosteller formula (9).

Statistical Analysis

Statistical analysis was performed using dedicated software (StatSoft Statistica, v. 12, Tulsa, OK). Continuous variables are presented as means ± SD, whereas categorical variables are reported as frequencies and percentages. Concerning LV EDVi, $LAVi_{max}$, 3D MA area, RV EDVi, $RAVi_{max}$, and 3-D TA area indices, individual values of athletes were normalized to the mean value of the control group to calculate their relative increase. After verifying the normal distribution of each variable using the Shapiro–Wilk test, athlete groups were compared with unpaired Student's *t* test or Mann–Whitney *U* test for continuous variables and chi-square or Fisher's exact test for categorical variables, as appropriate. Multiple-group comparisons were performed using ANOVA (with Fisher's post hoc test) or the Kruskal–Wallis test (with Dunn's post hoc test). The relative increase in the aforementioned parameters was compared using one-way repeated-measures ANOVA (with Fisher's post hoc test). The Pearson or Spearman test was computed to assess the correlation between continuous variables. Multivariate linear regression analysis was performed in athletes to find independent determinants of MA and TA 3-D area index. To avoid multicollinearity, tolerance was set at >0.4. A two-sided *P* value of <0.05 was considered as statistically significant. The intra- and interobserver variabilities were evaluated by intraclass correlation coefficient (ICC) values. To assess the intraobserver reproducibility of the presented key parameters, the experienced first operator (A.F.) of the off-line measurements repeated the 3-D analysis in a randomly selected subset of 5-5-5 subjects from each group blinded to previous results. The interobserver variability was deter-

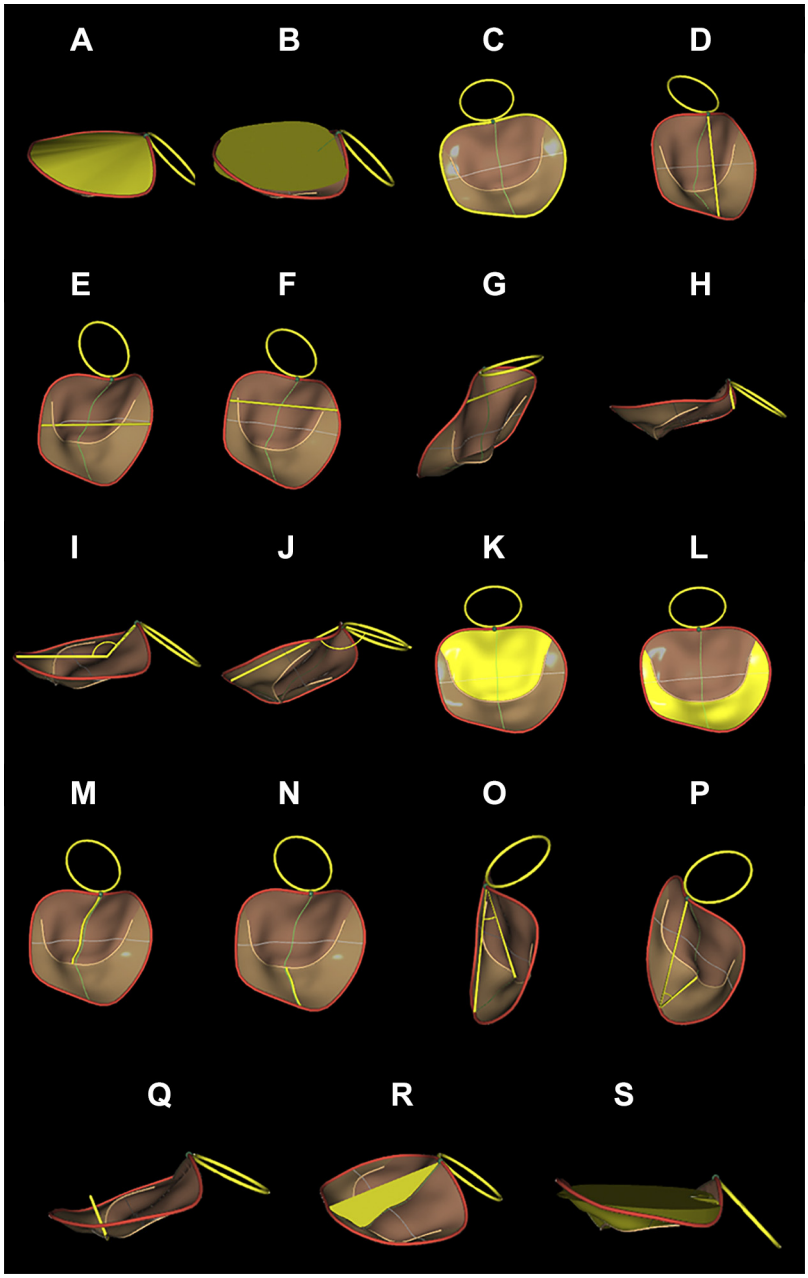

Figure 2. Graphical representation of the three-dimensional (3-D) echocardiography-derived measurements concerning the mitral valve. *A*: annulus 3-D area. The yellow surface represents the adjusted 3-D area of the mitral annulus. *B*: annulus two-dimensional (2-D) area. The yellow surface represents the projected area at the level of best-fit plane of the mitral annulus. *C*: annulus perimeter. The yellow line represents the circumference of the mitral annulus. *D*: anteroposterior diameter. The yellow line represents the distance between the anterior and posterior reference points of the mitral annulus. *E*: posteromedial-anterolateral diameter. The yellow line represents the longest distance between the posteromedial and the anterolateral reference points of the mitral annulus. *F*: commissural diameter. The yellow line represents the distance between the annular points at the level of the commissures. *G*: intertrigonal distance. The yellow line represents the distance between the points at which the anterior leaflet attached to the fibrous skeleton of the heart between trigones. *H*: annulus height. The yellow line represents the distance between the highest point and the lowest point of the mitral annulus. *I*: nonplanar angle. The angle enclosed by the two yellow lines is used to calculate the nonplanar angle that describes the saddle shape of the mitral annulus. *J*: mitral-aortic angle. The angle enclosed by the two yellow lines (axes of aortic and mitral annuli) is used to calculate the mitral-aortic angle. *K*: anterior leaflet area. The yellow surface represents the area of the anterior mitral valve leaflet. *L*: posterior leaflet area. The yellow surface represents the area of the posterior mitral valve leaflet. *M*: anterior leaflet length. The yellow line represents the central contour line from which leaflet length is calculated. *N*: posterior leaflet length. The yellow line represents the central contour line from which leaflet length is calculated. *O*: anterior leaflet angle. The angle enclosed by the two yellow lines is used to calculate the anterior mitral valve leaflet angle. *P*: posterior leaflet angle. The angle enclosed by the two yellow lines is used to calculate the posterior mitral valve leaflet angle. *Q*: tenting height. The highlighted yellow line shows the central maximal distance between the mitral annular plane and the leaflet coaptation point. *R*: tenting area. The highlighted yellow surface shows the maximal area between the mitral annular anteroposterior axis and the central leaflet coaptation point. *S*: tenting volume. The yellow surface represents the volume enclosed between the mitral annulus and the mitral valve leaflets.

mined by 3-D analysis of the same subjects by a second experienced operator (A.K.) in a blinded fashion.

RESULTS

Four hundred and twenty-five healthy athletes were identified with a previous echocardiographic examination with both left heart- and right heart-focused 3-D datasets. From this cohort, 42 (9.9%) athletes presented with at least mild MR. Eight athletes were excluded due to either suboptimal image quality for MA quantification (n = 6) or noncompatible image source vendor (n = 2). Thus, 34 athletes (male/female: 26/8) formed the final study population (MR athlete group). Furthermore, 34 age-matched athletes (non-MR athlete group) and 34 healthy, sedentary individuals (control group) with the same sex distribution (male/female: 26/8) were selected from our database (Fig. 4; Table 1).

Basic anthropometric, hemodynamic, and training specific data of the study groups are summarized in Table 1. Our athlete populations consisted of mixed or endurance-trained individuals, predominantly soccer players (28%), water polo players (28%), and swimmers (25%). Athletes had a higher height, weight, and lower resting heart rate than the sedentary control group. Athletes without MR demonstrated significantly higher systolic blood pressure compared with the other two groups. Athletes have been participating in competitive sports for an average of 15 years; at the time of the echocardiographic investigation, they trained an average of

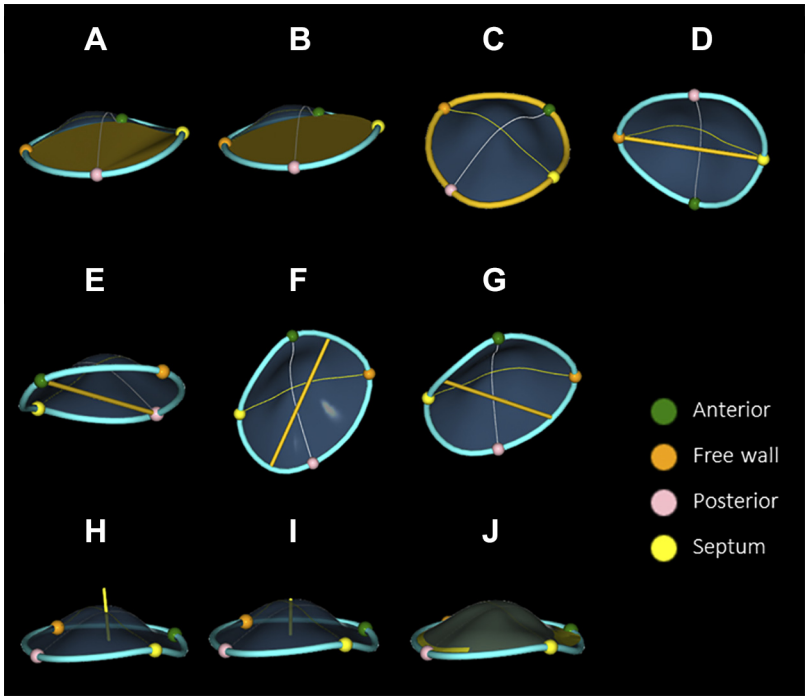

Figure 3. Graphical representation of the three-dimensional (3-D) echocardiography-derived measurements concerning the tricuspid valve. *A*: annulus 3-D area. The yellow surface represents the adjusted 3-D area of the tricuspid annulus. *B*: annulus two-dimensional (2-D) area. The yellow surface represents the projected area at the level of best-fit plane of the tricuspid annulus. *C*: annulus perimeter. The yellow line represents the circumference of the tricuspid annulus. *D*: 4-chamber diameter: The yellow line shows the distance between the free wall and the septal reference points. *E*: two-chamber diameter: The yellow line shows the distance between the anterior and the posterior reference points. *F*: major axis. The yellow line shows the maximal diameter of the tricuspid annulus. *G*: minor axis. The yellow line shows the minimal diameter of the tricuspid annulus. *H*: coaptation point height. The highlighted line represents the distance between the distal coaptation point of the tricuspid valve leaflets and the annular plane. *I*: max tenting height. The highlighted line represents the distance between the proximal coaptation point (tenting point) of the tricuspid valve leaflets and the annular plane. *J*: tenting volume. The yellow surface represents the volume enclosed between the tricuspid annulus and the tricuspid valve leaflets.

17 h/wk. BSA, heart rate, competitive years, weekly training hours, and CPET-derived peak exercise capacity did not differ between the two athlete groups (Table 1).

Conventional 2-D and 3-D echocardiographic parameters are shown in Table 2. As expected, there were significant differences between the athlete groups and the control group concerning LV and RV morphological and functional parameters. LV and RV EDVi and ESVi were significantly higher in the athletes compared with controls; on the other hand, these did not differ between the MR and non-MR athlete groups. LV Mi, LV SVi, and RV SVi values were the highest in the athlete group with MR compared with non-MR and control groups. LV EF, GLS, GCS, RV FAC, and RV EF showed significantly decreased resting values in the athletic groups than controls. Notably, LV GLS was higher in the MR athlete group compared with the non-MR group. TAPSE and RV septal and free wall longitudinal strain did not differ between groups. 3-D LA and RA maximal volume indices were higher among athletes with MR, even compared with non-MR athletes. In terms of LA reservoir and contractile function, there was no difference between the groups; however, LA passive EF referring to conduit function was significantly lower in the MR athlete group compared with controls. Although RA contractile function was similar, athlete groups presented with lower RA reservoir and conduit function. Moreover, RA total emptying fraction was significantly lower in the MR athlete group compared with non-MR athletes. Concerning diastolic function, there was no difference in either mitral inflow velocities or early diastolic mitral annular velocities between our study groups. In contrast, late diastolic annular velocities (a') were lower in athletes than in controls (Table 2).

In the MR athlete group, all individuals presented with mild MR, and no moderate regurgitation was established (VCW: 0.22 ± 0.07 cm). Interestingly, 74% of athletes with MR also had mild TR (VCW: 0.19 ± 0.07 cm). In the non-MR group, 9% of athletes presented with mild TR (VCW: 0.12 ± 0.04 cm).

We have compared the exercise-induced relative dilation of the LV, the LA, and the MA in the overall athlete cohort. Although the relative increase in LV EDVi and $LAVi_{max}$ was comparable, the MA 3-D area index's increment was disproportionately higher, with an average enlargement of over 60%. Concerning the right heart, the relative increase in the 3-D TA area index was significantly higher than in RVEDVi but showed no difference compared with $RAVi_{max}$. The increment in $RAVi_{max}$ was higher compared with RVEDVi (Fig. 5). We investigated the relative geometrical changes in female athletes (n = 16) separately and found that the increment in $LAVi_{max}$ (46 ± 33%) was significantly higher compared with LVEDVi (32 ± 21%) but was still lower than MA 3-D area index (61 ± 30%, overall $P < 0.001$). In terms of the right heart, the increment in TA 3-D area index (35 ± 25%) was similar to RVEDVi (35 ± 25%), but both were lower compared with $RAVi_{max}$ (49 ± 45%, overall $P < 0.001$).

The three groups differed significantly from each other with regard to all of the parameters (3-D and 2-D area indices, perimeter, anteroposterior, posteromedial-anterolateral, commissural diameters, intertrigonal distance) describing the size of the MA, as athletes having MR had significantly higher values even compared with athletes without MR (Table 3; Fig. 6). The athlete groups had higher annulus height and less obtuse mitral-aortic angle. Athletes without MR had a more pronounced MA saddle shape, as suggested by the significantly less obtuse nonplanar angle and higher annulus height to commissural width ratio (AHCWR, Fig. 6). Interestingly, athletes with MR were rather similar in this regard to sedentary controls. Sphericity, annular excursion, and MA area fraction did not differ between the athlete groups. Anterior leaflet length and area were significantly

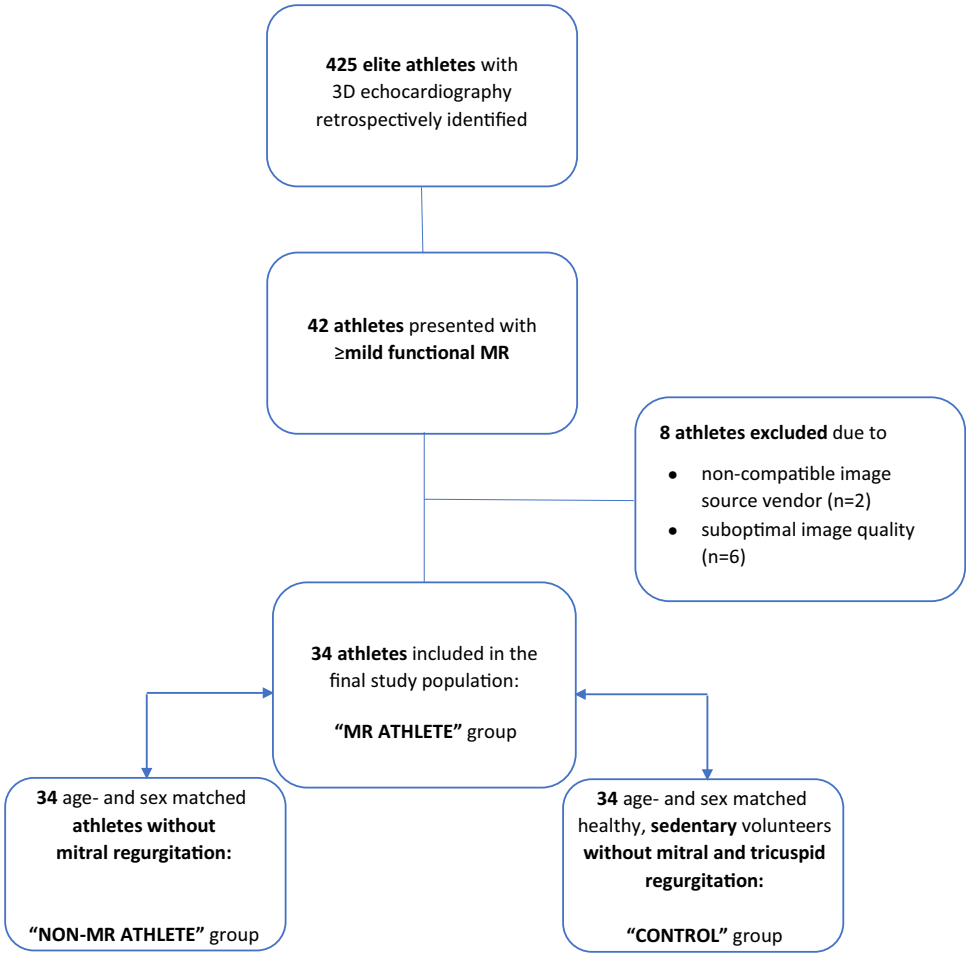

Figure 4. Flowchart for the identification of the study groups. MR, mitral regurgitation.

higher in the MR athletes even compared with non-MR athletes; however, posterior leaflet length and area did not show a difference between the two athlete groups. The anterior leaflet angle was significantly lower in the MR athlete group compared with non-MR athletes. Tenting height, area, and volume indices were higher in both athlete groups compared with the control group (Table 3; Fig. 6).

Interestingly, athletes with MR had also significantly enlarged TA, as shown by 3-D and 2-D area indices, four-chamber view diameters, and minor axis diameters compared

Table 1. *Baseline and training-specific characteristics of athlete and control groups*

	MR Athletes	Non-MR Athletes	Controls	Overall *P*
Subjects, *n*	34	34	34	
Baseline characteristics				
Age, yr	24.0 ± 7.3	22.5 ± 5.0	23.9 ± 6.4	0.449
Male, *n* (%)	26 (76.5)	26 (76.5)	26 (76.5)	1.000
Height, cm	180.0 ± 13.1*	182.1 ± 10.5*	173.7 ± 7.6§#	0.003
Weight, kg	76.2 ± 17.7	77.9 ± 16.0*	70.8 ± 14.8#	0.043
BSA, m^2	1.9 ± 0.3	2.0 ± 0.2*	1.8 ± 0.2#	0.043
SBP, mmHg	128.4 ± 14.7#	137.7 ± 13.3§*	123.8 ± 14.8#	<0.001
DBP, mmHg	76.3 ± 9.1#	81.1 ± 9.6§	76.8 ± 9.0	0.031
HR, beats/min	62.4 ± 10.5*	67.3 ± 12.0*	78.2 ± 12.7§#	<0.001
Training-specific characteristics				
Since, years	14.8 ± 6.1	14.9 ± 5.4	–	0.903
Training time, h/wk	17.1 ± 7.4	16.9 ± 8.1	–	0.915
$\dot{V}O_2$, L/min	4.0 ± 1.0	4.0 ± 0.9	–	0.902
$\dot{V}O_2$/kg, mL/kg/min	52.8 ± 6.5	51.6 ± 8.7	–	0.512

Continuous variables are means ± SD; categorical variables are reported as frequencies (%). *$P < 0.05$ vs. controls, #$P < 0.05$ vs. non-MR athletes, §$P < 0.05$ vs. MR athletes. BSA, body surface area; DBP, diastolic blood pressure; HR, heart rate; MR, mitral regurgitation; SBP, systolic blood pressure; $\dot{V}O_2$, peak oxygen uptake; $\dot{V}O_2$/kg, peak oxygen uptake indexed to body weight.

Table 2. *Conventional 2-D and 3-D echocardiographic parameters of athlete and control groups*

	MR Athletes	Non-MR Athletes	Controls	Overall *P*
Subjects, *n*	34	34	34	
Left ventricular parameters				
LVIDd, mm	52.7 ± 5.9*	52.7 ± 4.6*	47.3 ± 4.4§#	0.001
IVSd, mm	10.6 ± 2.1*	10.1 ± 1.8	9.0 ± 1.5§	0.025
PWd, mm	9.1 ± 1.5*	9.0 ± 1.2*	7.8 ± 1.2§#	0.006
LV EDVi, mL/m^2	85.5 ± 17.2*	78.5 ± 11.8*	60.9 ± 12.1§#	<0.001
LV ESVi, ml/m^2	37.7 ± 10.5*	35.7 ± 7.8*	24.7 ± 5.7§#	<0.001
LV SVi, mL/m^2	47.8 ± 8.0*#	42.8 ± 5.5§*	36.2 ± 7.3§#	<0.001
LV Mi, g/m^2	89.4 ± 16.7*#	81.9 ± 12.6§*	64.9 ± 10.0§#	<0.001
LV EF, %	56.4 ± 4.8*	54.8 ± 4.5*	59.5 ± 3.8§#	<0.001
LV GLS, %	−19.4 ± 2.4*#	−18.3 ± 2.3§*	−20.6 ± 2.1§#	<0.001
LV GCS, %	−27.6 ± 3.2*	−26.6 ± 2.9*	−30.0 ± 2.8§#	<0.001
Left atrial, diastolic function and tissue-Doppler parameters				
2D LA ESVi, mL/m^2	31.7 ± 7.4*#	27.3 ± 7.4§*	22.4 ± 7.1§#	<0.001
$LAVi_{max}$, mL/m^2	37.1 ± 7.1*#	31.9 ± 6.2§*	24.7 ± 6.9§#	<0.001
$LAVi_{min}$, mL/m^2	15.3 ± 4.3*	13.5 ± 4.5*	9.6 ± 3.7§#	<0.001
$LAVi_{preA}$, mL/m^2	23.6 ± 5.9*#	19.2 ± 4.1§*	14.6 ± 4.8§#	<0.001
LA total EF, %	58.9 ± 7.5	59.1 ± 5.9	61.2 ± 7.9	0.361
LA passive EF, %	36.7 ± 7.9*	39.6 ± 6.6	40.8 ± 7.5§	0.041
LA active EF, %	35.0 ± 9.7	29.9 ± 14.4	34.4 ± 11.4	0.167
E, cm/s	90.1 ± 20.2	84.1 ± 22.3	87.2 ± 18.3	0.487
A, cm/s	53.2 ± 12.6	55.7 ± 13.3	62.0 ± 14.3	0.149
E/*A*	1.7 ± 0.4	1.6 ± 0.6	1.5 ± 0.4	0.096
DT, ms	162.1 ± 31.0	165.6 ± 32.5	173.2 ± 33.2	0.422
Mitral lateral *s*′, cm/s	11.3 ± 2.1*	11.9 ± 2.0	13.1 ± 2.9§	0.041
Mitral lateral *e*′, cm/s	18.8 ± 2.9	17.3 ± 3.6	18.3 ± 3.9	0.376
Mitral lateral *a*′, cm/s	7.5 ± 1.5*	7.1 ± 1.6*	8.7 ± 2.1§#	0.003
Mitral medial *s*′, cm/s	9.1 ± 1.1*	9.7 ± 1.2	10.2 ± 1.8§	0.028
Mitral medial *e*′, cm/s	13.3 ± 1.8	13.1 ± 2.5	14.5 ± 2.9	0.184
Mitral medial *a*′, cm/s	7.4 ± 1.7*	7.7 ± 1.6*	8.7 ± 1.8§#	0.007
E/*e*′ average	5.8 ± 1.3	5.7 ± 1.1	5.4 ± 1.3	0.669
Right ventricular parameters				
RVd, mm	35.0 ± 3.7*	34.6 ± 3.8*	30.1 ± 3.8§#	<0.001
RV EDVi, mL/m^2	84.9 ± 16.7*	79.1 ± 13.1*	61.2 ± 10.6§#	<0.001
RV ESVi, mL/m^2	38.0 ± 9.5*	35.9 ± 8.5*	25.1 ± 5.0§#	<0.001
RV SVi, mL/m^2	46.9 ± 8.4*#	43.2 ± 6.2§*	36.1 ± 6.7§#	<0.001
RVSP, mmHg	23.4 ± 4.8	24.7 ± 3.2*	20.6 ± 4.7#	<0.001
RV EF, %	55.5 ± 4.0*	55.1 ± 4.8*	58.9 ± 4.2§#	<0.001
TAPSE, mm	24.3 ± 3.9	24.0 ± 4.2	24.2 ± 3.5	0.907
FAC, %	49.9 ± 4.8*	49.5 ± 4.7*	53.1 ± 5.2§#	0.005
RVSLS, %	−21.0 ± 4.4	−21.9 ± 3.3	−21.5 ± 4.3	0.646
RVFWLS, %	−29.4 ± 3.5	−29.5 ± 2.7	−30.7 ± 4.0	0.262
Right atrial and tissue-Doppler parameters				
2D RA ESVi, mL/m^2	35.0 ± 8.4*#	29.1 ± 6.9§*	24.4 ± 6.9§#	<0.001
$RAVi_{max}$, mL/m^2	42.0 ± 9.7*#	35.1 ± 7.1§*	26.7 ± 6.2§#	<0.001
$RAVi_{min}$, mL/m^2	20.7 ± 6.4*#	16.0 ± 4.7§*	10.5 ± 3.3§#	<0.001
$RAVi_{preA}$, mL/m^2	28.3 ± 7.6*#	22.5 ± 5.1§*	15.3 ± 4.1§#	<0.001
RA total EF, %	50.9 ± 8.2*#	55.3 ± 8.8§*	60.2 ± 10.1§#	<0.001
RA passive EF, %	32.9 ± 8.1*	36.0 ± 7.0*	42.7 ± 10.0§#	<0.001
RA active EF, %	27.0 ± 8.2	28.8 ± 10.6	30.8 ± 10.6	0.296
Tricuspid annular *s*′, cm/s	13.2 ± 2.3*	13.1 ± 2.3*	15.0 ± 2.8§#	0.003
Tricuspid annular *e*′, cm/s	14.5 ± 3.4	14.4 ± 3.3	16.5 ± 3.4	0.123
Tricuspid annular *a*′, cm/s	9.2 ± 3.0*	9.6 ± 2.5*	13.2 ± 4.8§#	<0.001

Continuous variables are means ± SD; categorical variables are reported as frequencies (%). *$P < 0.05$ vs. controls, #$P < 0.05$ vs. non-MR athletes, §$P < 0.05$ vs. MR athletes. *A*, mitral inflow velocity during atrial contraction; *a*′, peak late (atrial) diastolic annular velocity; DT, deceleration time; *E*, early diastolic mitral inflow velocity; *e*′, early diastolic annular velocity; EDVi, end-diastolic volume index; EF, ejection fraction; ESVi, end-systolic volume index; FAC, fractional area change; GCS, global circumferential strain; GLS, global longitudinal strain; IVSd, interventricular septal thickness at end-diastole; LA, left atrium; LA active EF, LA active emptying fraction; LA passive EF, LA passive emptying fraction; LA total EF, LA total emptying fraction; $LAVi_{max}$, left atrial maximal volume index; $LAVi_{min}$, left atrial minimal volume index; $LAVi_{preA}$, left atrial preA wave volume index; LV, left ventricle; LVIDd, LV internal diameter at end-diastole; Mi, mass index; MR, mitral regurgitation; PWd, posterior wall thickness at end-diastole; RA, right atrium; RA active EF, RA active emptying fraction; RA passive EF, RA passive emptying fraction; RA total EF, RA total emptying fraction; $RAVi_{max}$, right atrial maximal volume index; $RAVi_{min}$, right atrial minimal volume index; $RAVi_{preA}$, right atrial preA wave volume index; RV, right ventricle; RVd, RV basal diameter; RVFWLS, RV free wall longitudinal strain; RVSLS, RV septal longitudinal strain; RVSP, right ventricular systolic pressure; *s*′, systolic annular velocity; SVi, stroke volume index; TAPSE, tricuspid annular plane systolic excursion; 2-D, two-dimensional; 3-D, three-dimensional.

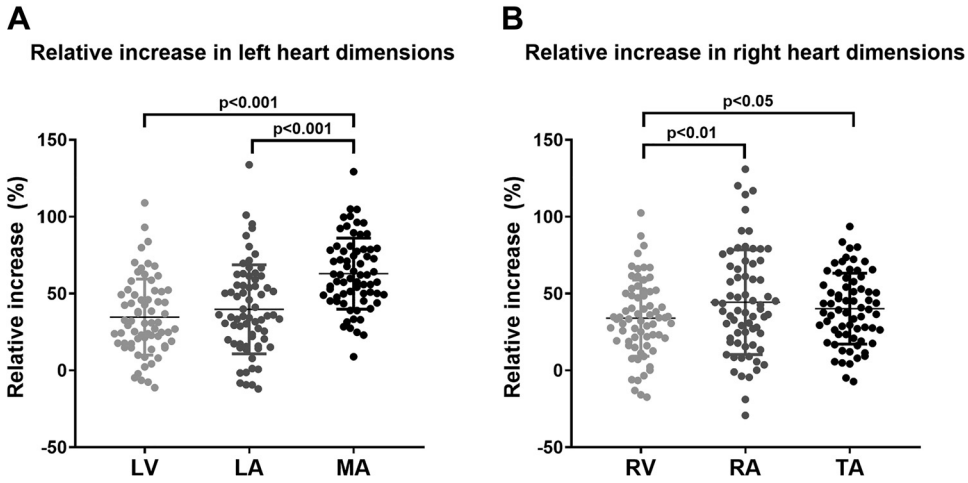

Figure 5. Comparison of the exercise-induced dilation of the left ventricle (LV), the left atrium (LA), and the mitral annulus (MA) (*A*) and the right ventricle (RV), the right atrium (RA), and the tricuspid annulus (TA) (*B*). Three-dimensional (3-D) MA area index showed a disproportionate increment compared with both LV and LA volume indices ($n = 68$, overall $P < 0.001$). The relative increase in the 3-D TA area index was significantly higher compared with RV volume index ($n = 68$, overall $P < 0.01$).

with both non-MR athletes and controls (Table 4 and Fig. 7). TA perimeter, two-chamber view diameters, and major axis diameters were comparable between athlete groups but still larger than controls. TA sphericity, area fraction, and systolic excursion were similar between groups. Maximal tenting height and tenting volume index were significantly higher in the athlete groups compared with the sedentary controls (Table 4; Fig. 7).

In the pooled population ($n = 102$), MA 3-D area index correlated with LV EDVi ($r = 0.704$, $P < 0.001$), LV Mi ($r = 0.657$, $P < 0.001$), and $LAVi_{max}$ ($r = 0.719$, $P < 0.001$), whereas TA 3-D area index correlated with RV EDVi ($r = 0.643$, $P < 0.001$) and $RAVi_{max}$ ($r = 0.741$, $P < 0.001$). MA tenting volume index correlated with LV EDVi ($r = 0.673$, $P < 0.001$), whereas TA tenting volume index correlated with RV EDVi ($r = 0.617$, $P < 0.001$). Furthermore, in athletes ($n = 68$), MA and TA 3-D area index correlated with $\dot{V}O_2$/kg (MA: $r = 0.443$, $P < 0.001$; TA: $r = 0.423$, $P < 0.01$). Multivariate linear regression models were built to identify independent determinants of MA and TA 3-D area index in athletes. In the first model (comprising age, sex, LVEDVi, $LAVi_{max}$, and $\dot{V}O_2$/kg), $LAVi_{max}$ and $\dot{V}O_2$/kg were found to be independent determinants of MA 3-D area index, with a cumulative R value of 0.681 ($P < 0.001$; Table 5). In a second model (comprising age, sex, RVEDVi,

Table 3. *Mitral valve quantification of athlete and control groups*

	MR Athletes	Non-MR Athletes	Controls	Overall *P*
Subjects, *n*	34	34	34	
Annulus				
Annulus 3-D area index, cm^2/m^2	8.2 ± 1.0*#	7.2 ± 1.0§*	4.7 ± 0.6§#	<0.001
Annulus 2-D area index, cm^2/m^2	7.3 ± 0.9*#	6.4 ± 0.9§*	4.2 ± 0.6§#	<0.001
Annulus perimeter, cm	14.2 ± 1.2*#	13.6 ± 1.1§*	10.6 ± 0.9§#	<0.001
A-P diameter, cm	3.6 ± 0.4*#	3.4 ± 0.4§*	2.7 ± 0.4§#	<0.001
PM-AL diameter, cm	4.5 ± 0.4*#	4.3 ± 0.4§*	3.4 ± 0.3§#	<0.001
Commissural diameter, cm	4.5 ± 0.4*#	4.2 ± 0.4§*	3.4 ± 0.3§#	<0.001
Intertrigonal distance, cm	3.3 ± 0.6*#	2.9 ± 0.4§*	2.4 ± 0.4§#	<0.001
Sphericity index	0.8 ± 0.1	0.8 ± 0.1	0.8 ± 0.1	0.312
Annulus height, mm	9.6 ± 2.8*	10.5 ± 2.1*	7.2 ± 2.0§#	<0.001
Nonplanar angle, °	128.9 ± 16.9#	116.0 ± 21.4§*	131.1 ± 13.8#	<0.001
Mitral annular excursion, mm	12.9 ± 2.0*	12.2 ± 2.1	11.3 ± 2.1§	0.009
Annulus (2-D) area fraction, %	−4.8 ± 6.5	−2.5 ± 3.9	−4.1 ± 9.0	0.371
Mitral-aortic angle, °	140.4 ± 13.1*	138.1 ± 12.1*	147.1 ± 11.6§#	0.011
AHCWR, %	21.8 ± 6.8#	25.2 ± 5.6§*	21.6 ± 6.7#	0.036
Leaflets				
Anterior leaflet area index, cm^2/m^2	4.4 ± 0.9*#	3.4 ± 0.5§*	2.5 ± 0.4§#	<0.001
Posterior leaflet area index, cm^2/m^2	4.2 ± 0.8*	4.3 ± 0.8*	2.6 ± 0.5§#	<0.001
Anterior leaflet length, cm	2.7 ± 0.3*#	2.5 ± 0.3§*	2.0 ± 0.3§#	<0.001
Posterior leaflet length, cm	1.7 ± 0.3*	1.8 ± 0.4*	1.4 ± 0.3§#	<0.001
Anterior leaflet angle, °	23.9 ± 4.6#	26.3 ± 6.0§	25.1 ± 4.8	0.043
Posterior leaflet angle, °	39.5 ± 9.9	39.6 ± 7.6	40.6 ± 10.2	0.948
Tenting height, cm	1.0 ± 0.2*	1.0 ± 0.2*	0.8 ± 0.2§#	<0.001
Tenting area index, cm^2/m^2	1.2 ± 0.3*	1.2 ± 0.3*	0.8 ± 0.2§#	<0.001
Tenting volume index, mL/m^2	2.0 ± 0.6*	1.8 ± 0.6*	0.9 ± 0.3§#	<0.001

Continuous variables are means ± SD; categorical variables are reported as frequencies (%). *$P < 0.05$ vs. controls, #$P < 0.05$ vs. non-MR athletes, §$P < 0.05$ vs. MR athletes. AHCWR, annulus height to commissural width ratio; A-P diameter, anteroposterior diameter; MR, mitral regurgitation; PM-AL diameter, posteromedial-anterolateral diameter; 2-D, two-dimensional; 3-D, three-dimensional.

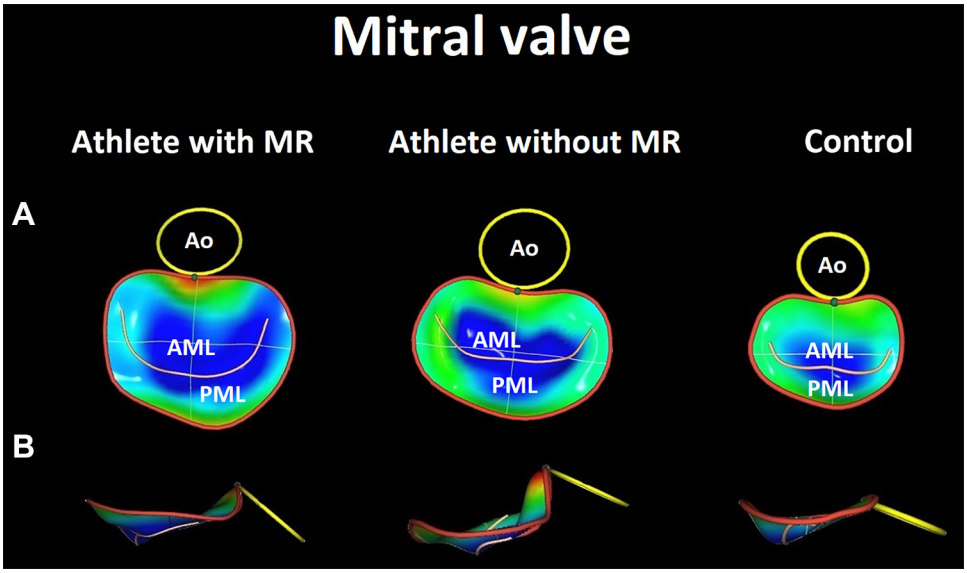

Figure 6. Three-dimensional (3-D) mitral annular reconstructions of athletes with and without mitral regurgitation (MR) and a healthy sedentary volunteer (control; representative cases). The impact of regular exercise training is represented by the larger dimensions of the mitral annulus in athletes; however, athletes presented with MR even had a larger annular size. Athletes without MR had a more pronounced saddle shape, whereas athletes with MR and controls did not differ in this regard. See details in the text. *A*: surgeon's view. *B*: side view of the mitral annulus. More blueish hues represent more tenting of the mitral valve leaflets. AML, anterior mitral valve leaflet; Ao, aortic annulus; PML, posterior mitral valve leaflet.

$RAVi_{max}$, and $\dot{V}O_2$/kg), $RAVi_{max}$ was the only independent predictor of TA 3-D area index, with a cumulative *R* value of 0.648 ($P < 0.001$; Table 5).

Despite using transthoracic 3-D echocardiographic images for annular quantification, good intra- and interobserver variabilities could be assessed concerning all of the key measurements (intraobserver and interobserver ICC values with 95% confidence intervals, respectively; MA 3-D area: 0.978 [0.949–0.991] and 0.961 [0.909–0.984], nonplanar angle: 0.842 [0.656–0.933] and 0.778 [0.534–0.903], MA tenting volume: 0.977 [0.945–0.991] and 0.944 [0.868–0.977], TA 3-D area: 0.973 [0.926–0.990] and 0.941 [0.863–0.976], TA tenting volume: 0.957 [0.898–0.982] and 0.884 [0.740–0.952]). These results are similar to those reported in previous publications (10, 11).

DISCUSSION

To the best of our knowledge, our study is the first to characterize the annular geometry of mitral and tricuspid valves in elite athletes using 3-D echocardiography. We have found that exercise-induced remodeling comprises a significant dilation of annular dimensions and increased leaflet tenting of both atrioventricular valves. MA showed a disproportionate enlargement compared with both the LV and the LA, whereas TA was more extensively increased than the RV. Moreover, we have demonstrated a more pronounced saddle shape of the MA in athletes without MR, which was not present in those athletes who had mild MR.

The mitral and tricuspid annuli are the fibrous continuity between ventricular and atrial myocardium and leaflet tissues. These saddle-shaped structures' function is to minimize leaflet stress and optimize coaptation throughout the corresponding phase of the cardiac cycle (12). 3-D echocardiography revolutionized our understanding of the MA geometry and dynamics, highlighting important pathophysiological differences between primary and secondary mitral valve diseases. Although MA dilation can be present both in patients with mitral valve prolapse (Barlow disease or fibroelastic

Table 4. *Tricuspid valve quantification of athlete and control groups*

	MR Athletes	Non-MR Athletes	Controls	Overall *P*
Subjects, *n*	34	34	34	
Annulus				
Annulus 3-D area index, cm^2/m^2	7.2 ± 1.1*#	6.5 ± 1.1§*	5.0 ± 0.8§#	<0.001
Annulus 2-D area index, cm^2/m^2	7.1 ± 1.1*#	6.4 ± 1.1§*	4.9 ± 0.8§#	<0.001
Annulus (2-D) area fraction, %	15.2 ± 4.4	15.4 ± 4.0	16.1 ± 4.2	0.622
Annulus perimeter, cm	13.3 ± 1.2*	12.9 ± 1.2*	10.8 ± 0.8§#	<0.001
4-chamber diameter, cm	4.1 ± 0.3*#	3.8 ± 0.4§*	3.2 ± 0.3§#	<0.001
2-chamber diameter, cm	4.1 ± 0.4*	4.0 ± 0.4*	3.2 ± 0.4§#	<0.001
Major axis, cm	4.4 ± 0.5*	4.3 ± 0.5*	3.6 ± 0.3§#	<0.001
Minor axis, cm	3.9 ± 0.4*#	3.7 ± 0.3§*	3.1 ± 0.3§#	<0.001
Sphericity index	0.9 ± 0.1	0.9 ± 0.1	0.9 ± 0.1	0.712
Excursion, cm	1.6 ± 0.2	1.5 ± 0.3	1.5 ± 0.3	0.370
Leaflets				
Max tenting height, cm	0.9 ± 0.1*	1.0 ± 0.2*	0.7 ± 0.1§#	<0.001
Tenting volume index, mL/m^2	2.1 ± 0.5*	2.0 ± 0.6*	1.0 ± 0.3§#	<0.001

Continuous variables are means ± SD; categorical variables are reported as frequencies (%). *$P < 0.05$ vs. controls, #$P < 0.05$ vs. non-MR athletes, §$P < 0.05$ vs. MR athletes. MR, mitral regurgitation; 2-D, two-dimensional; 3-D, three-dimensional.

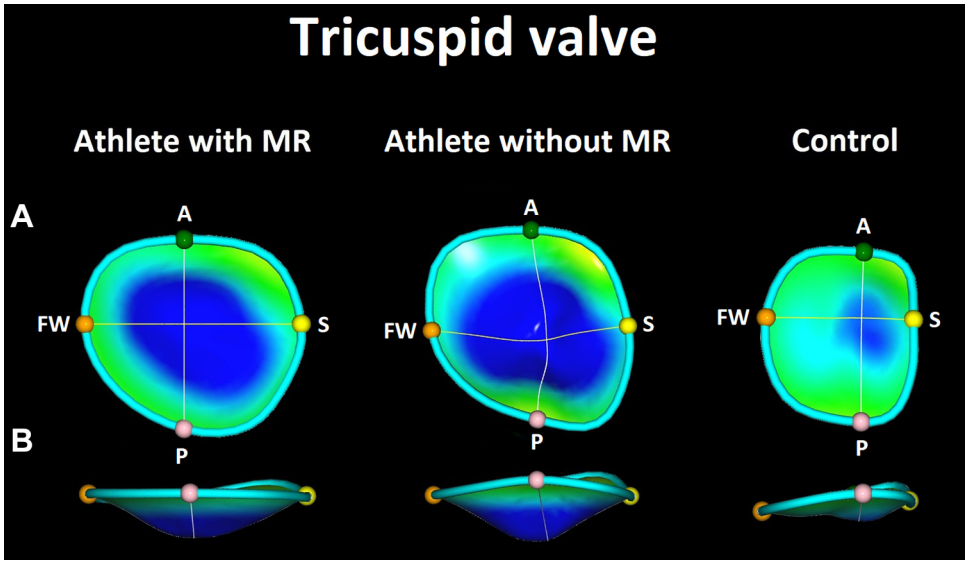

Figure 7. Three-dimensional (3-D) tricuspid annular reconstructions of athletes with and without mitral regurgitation (MR) and a healthy sedentary volunteer (control; representative cases). The impact of regular exercise training is represented by the larger dimensions of the tricuspid annulus in athletes; however, athletes presented with MR even had a larger annular size. See details in the text. *A*: surgeon's view. *B*: side view of the tricuspid annulus. More blueish hues represent more tenting of the tricuspid valve leaflets. A, anterior; FW, free wall; P, posterior; S, septal reference points.

deficiency) and in patients with ventricular functional MR, the latter group is rather characterized by a stiff, hypodynamic MA. The flattening of the saddle-shaped MA is also considered as an adverse response to different pathological stimuli (11, 12). The added value of 3-D echocardiography is evident not just in terms of describing the nonplanar MA geometry and eliminating the underestimation of MA size (when assessed by linear measurements) but also in the more accurate quantification of MR and supporting a more personalized diagnostic approach and subsequent therapeutic decisions (11). Recently, 3-D modeling and systolic tracking of the TA became available using 3-D echocardiography, and it promises similar advantages compared with conventional assessment (13).

Table 5. *Multivariate linear regression analysis: independent determinants of MA 3-D area index and TA 3-D area index in athletes (n = 68)*

Covariate	β	*P*
MA 3-D area index		
Age	0.153	0.124
Sex	0.156	0.156
$LAVi_{max}$	**0.398**	**0.001**
LV EDVi	0.200	0.131
$\dot{V}O_2$/kg	**0.260**	**0.033**
Cumulative *R*	0.681	
Standard error	1.13	
Cumulative *P*	0.000001	
TA 3-D area index		
Age	−0.040	0.719
Sex	0.117	0.299
$RAVi_{max}$	**0.543**	**<0.001**
RV EDVi	0.013	0.932
$\dot{V}O_2$/kg	0.221	0.108
Cumulative *R*	0.648	
Standard error	1.19	
Cumulative *P*	0.000005	

Boldface indicates significant beta values. EDVi, end-diastolic volume index; $LAVi_{max}$, left atrial maximal volume index; LV, left ventricle; MA, mitral annular; $RAVi_{max}$, right atrial maximal volume index; RV, right ventricle; TA, tricuspid annular; $\dot{V}O_2$/kg, peak oxygen uptake indexed to body weight; 3-D, three-dimensional.

Regular physical exercise exposes the cardiovascular system to often extreme hemodynamic demands, resulting in significant changes in cardiac morphology and function (14). Although the ventricular myocardium's dynamic adaptation is definitely the most widely known aspect when considering an athlete's heart, alterations of the interconnected valvular apparatus should not be overlooked. During intense exercise, the atrioventricular valves have to support an adequate diastolic filling while also keeping their systolic competency to maintain the "one-way" circulation in the face of a wide range of intracardiac pressures and ventricular outputs (15).

Still, data are scarce even concerning MA and TA linear dimensions in athletes. In accordance with our current results, it was previously shown that athletes have significantly higher MA linear diameters than sedentary controls. Moreover, a more pronounced MA enlargement exists in athletes presenting with MR (5). Although functional mitral and tricuspid regurgitation rarely exceed the mild degree in athletes, a higher overall prevalence of MR and TR is reported in the literature (5). In our cohort, the vast majority of athletes with functional MR had concomitant TR, and interestingly, the MR group is presented with higher TA dimensions as well. This phenomenon implies that athletes prone to more excessive dilation of the MA are susceptible to a more pronounced TA remodeling. Of note, it has been suggested that alterations in TA geometry can be present even in the case of degenerative processes affecting the MA primarily (16). The mitral valve apparatus also shows a distinct change in shape if we compare the two athlete groups: although in athletes with MR, the parameters referring to the MA saddle shape, namely, annulus height to commissural width ratio (AHCWR) and nonplanar angle, were comparable with the values of sedentary controls, increased AHCWR and a less obtuse nonplanar angle were found in athletes without MR. These latter indicate a more pronounced MA saddle shape in that group, which is, according to our knowledge, a unique finding across the spectrum of physiological or pathophysiological

alterations of the MA (11). However, the anatomical advantages of this phenomenon are not completely clear. We may hypothesize that it may serve as an adaptive change to maintain proper coaptation during the different exercise levels when chamber geometry and intracardiac pressures continuously change. The MA nonplanarity of athletes presented with MR did not significantly differ from sedentary controls, suggesting that in this population, the mild regurgitation may originate at least partially from the "insufficient" geometrical adaptation of the MA to regular, intense exercise. Interestingly, the anterior leaflet area, but not posterior leaflet area, was significantly higher in athletes with MR compared with those without. According to previous data, mechanical stretch by papillary muscle displacement can induce leaflet hyperplasia (17). However, as the enlargement of the leaflets is usually proportional in pathological states, the asymmetrical growth of the mitral valve leaflets may be a specific manifestation of this "adverse" athletic adaptation accompanied by MR.

Athletes with MR showed tendentially higher LV volumes; significantly higher LV GLS, $LAVi_{max}$, and $RAVi_{max}$; and significantly lower RA total emptying fraction than athletes with no MR. Although such mild MR (assessed during resting conditions) certainly cannot be considered a hemodynamically relevant stimulus, these observations refer to what can be seen in the case of pathological LV volume overload (18, 19). These findings can originate in two ways: *1*) an athlete with a predisposition to a more pronounced exercise-induced chamber dilation may also be more prone to higher MA dimensions and a consequential MR, and *2*) there is an inherent anatomical cause of the MR that may significantly increase during exercise, resulting in more excessive cardiac remodeling. Nevertheless, further studies involving stress echocardiography are warranted to clarify this classical "chicken or the egg" dilemma. In accordance with our previous publication (2), we found a relatively more pronounced biatrial dilation in female athletes. Future studies with higher case numbers should also target sex differences in this regard.

MA and TA areas showed at least moderate correlations with the corresponding ventricular and atrial volumes, confirming these exercise-induced dilatative processes' interconnected nature. A modest but significant increase in the tenting volumes of both atrioventricular valves could also be demonstrated, related to the ventricular volumes. Accordingly, a mixed type of functional MR and TR (showing the characteristics of both atrial and ventricular types) was established in our examined cohort of athletes. MA and TA 3-D areas also correlated with CPET-derived exercise performance; in the case of the MA, $\dot{V}O_2$/kg was even found to be an independent determinant. These findings rather support that the atrioventricular annular dilation is still one of the adaptive aspects of the complex physiological cardiac response to regular, intense exercise training. Notably, however, atrial volumes were independent determinants of annular areas, whereas ventricular volumes were not. These results resonate with recent publications showing that the RA dilation is the major determinant of TA size in patients with atrial fibrillation and/or functional TR (20, 21). Longitudinal studies with long-term follow-up are required to establish the (patho)physiological link between exercise-induced cardiac remodeling, functional valvular regurgitation, and, eventually, occurrence of atrial fibrillation.

Limitations

Several limitations have to be acknowledged. First, the study cohort's size is relatively limited, mainly because we aimed to investigate elite athletes with available good-quality 3-D acquisitions and presenting with MR and compare them with those without. Second, clinical relevance and therapeutic consequences of such quantifications would be related to athletes with primary valvular heart diseases and higher grades of regurgitation; however, athletes with such disorders were absent in our database. Nevertheless, we plan a long-term follow-up of our athletes to investigate the progression/regression dynamics of the established alterations and the potential occurrence of clinical adverse events. 3-D echocardiographic quantification of the mitral valve is primarily designed for transesophageal images, where spatial and temporal resolutions are higher. However, athletes are generally presenting with exceptionally good acoustic windows, and data have shown that results derived from transthoracic and transesophageal approaches are rather interchangeable (8). Intraobserver and interobserver variability also confirmed the reliability of our measurements. The generalizability of our results to other sport disciplines, to amateur athletes, and to different age categories remains unknown.

Conclusions

In our retrospective cohort study of young elite athletes, we have shown that beyond the dilation of the cardiac chambers, atrioventricular annuli may undergo a disproportionate remodeling in response to regular, intense exercise training. Athletic valvular adaptation is characterized by both annular enlargement and increased leaflet tenting of both the mitral and tricuspid valves. There are also specific differences in MA geometry between athletes presented with or without functional MR. Further research is warranted in athletes competing in other sport disciplines, in master athletes, and in athletes with primary valvular heart diseases.

GRANTS

This study was partly financed by the National Research, Development and Innovation Office of Hungary (NKFIA; NVKP_16-1-2016-0017 National Heart Program). The research was partly financed by the Thematic Excellence Program (Tématerületi Kiválósági Program, 2020-4.1.1.-TKP2020) of the Ministry for Innovation and Technology in Hungary, within the framework of the Therapeutic Development and Bioimaging programmes of the Semmelweis University. The research was also supported by the ÚNKP-20-5 and the ÚNKP-20-3-II New National Excellence Program of the Ministry for Innovation and Technology from the source of the National Research, Development and Innovation Fund. This project was also supported by a grant from the National Research, Development and Innovation Office (NKFIH) of Hungary (K135076 to B.M.). A. Kovács was supported by the János Bolyai Research Scholarship of the Hungarian Academy of Sciences. A. Kovács was also supported by GE Vingmed Ultrasound (Horten, Norway) by a research grant permitting the use of 4D Auto TVQ software.

DISCLOSURES

No conflicts of interest, financial or otherwise, are declared by the authors.

AUTHOR CONTRIBUTIONS

A.F., B.K.L., M.T., A.S., O.K., B.M., and A.K. conceived and designed research; A.F., M.T., and A.K. performed experiments; A.F., B.K.L., M.T., E.C., E.K., and A.K. analyzed data; A.F., B.K.L., M.T., N.S., A.S., O.K., and A.K. interpreted results of experiments; A.F. and B.K.L. prepared figures; A.F., B.K.L., and A.K. drafted manuscript; A.F., B.K.L., M.T., A.R.K., N.S., E.C., E.K., M.B., A.S., O.K., B.M., and A.K. edited and revised manuscript; A.F., B.K.L., M.T., A.R.K., N.S., E.C., E.K., M.B., A.S., O.K., B.M., and A.K. approved final version of manuscript.

REFERENCES

1. **Olah A**, **Kovacs A**, **Lux A**, **Tokodi M**, **Braun S**, **Lakatos BK**, **Matyas C**, **Kellermayer D**, **Ruppert M**, **Sayour AA**, **Barta BA**, **Merkely B**, **Radovits T.** Characterization of the dynamic changes in left ventricular morphology and function induced by exercise training and detraining. *Int J Cardiol* 277: 178–185, 2019. doi:10.1016/j.ijcard.2018.10.092.
2. **Lakatos BK**, **Molnar AA**, **Kiss O**, **Sydo N**, **Tokodi M**, **Solymossi B**, **Fabian A**, **Dohy Z**, **Vago H**, **Babity M**, **Bognar C**, **Kovacs A**, **Merkely B.** Relationship between cardiac remodeling and exercise capacity in elite athletes: incremental value of left atrial morphology and function assessed by three-dimensional echocardiography. *J Am Soc Echocardiogr* 33: 101–109.e1, 2020. doi:10.1016/j.echo.2019.07.017.
3. **Muraru D**, **Guta AC**, **Ochoa-Jimenez RC**, **Bartos D**, **Aruta P**, **Mihaila S**, **Popescu BA**, **Iliceto S**, **Basso C**, **Badano LP.** Functional regurgitation of atrioventricular valves and atrial fibrillation: an elusive pathophysiological link deserving further attention. *J Am Soc Echocardiogr* 33: 42–53, 2020. doi:10.1016/j.echo.2019.08.016.
4. **Cavarretta E**, **Peruzzi M**, **Versaci F**, **Frati G**, **Sciarra L.** How to manage an athlete with mitral valve prolapse. *Eur J Prev Cardiol*, 2020 Jul 30 (online ahead of print). doi:10.1177/2047487320941646.
5. **Gjerdalen GF**, **Hisdal J**, **Solberg EE**, **Andersen TE**, **Radunovic Z**, **Steine K.** Atrial size and function in athletes. *Int J Sports Med* 36: 1170–1176, 2015. doi:10.1055/s-0035-1555780.
6. **Lang RM**, **Badano LP**, **Mor-Avi V**, **Afilalo J**, **Armstrong A**, **Ernande L**, **Flachskampf FA**, **Foster E**, **Goldstein SA**, **Kuznetsova T**, **Lancellotti P**, **Muraru D**, **Picard MH**, **Rietzschel ER**, **Rudski L**, **Spencer KT**, **Tsang W**, **Voigt JU.** Recommendations for cardiac chamber quantification by echocardiography in adults: an update from the American Society of Echocardiography and the European Association of Cardiovascular Imaging. *J Am Soc Echocardiogr* 28: 1–39.e14, 2015. doi:10.1016/j.echo.2014.10.003.
7. **Zoghbi WA**, **Adams D**, **Bonow RO**, **Enriquez-Sarano M**, **Foster E**, **Grayburn PA**, **Hahn RT**, **Han Y**, **Hung J**, **Lang RM**, **Little SH**, **Shah DJ**, **Shernan S**, **Thavendiranathan P**, **Thomas JD**, **Weissman NJ.** Recommendations for noninvasive evaluation of native valvular regurgitation: a report from the American Society of Echocardiography developed in collaboration with the society for cardiovascular magnetic resonance. *J Am Soc Echocardiogr* 30: 303–371, 2017. doi:10.1016/j.echo.2017.01.007.
8. **Aruta P**, **Muraru D**, **Guta AC**, **Mihaila S**, **Ruozi N**, **Palermo C**, **Elnagar B**, **Iliceto S**, **Badano LP.** Comparison of mitral annulus geometry between patients with ischemic and non-ischemic functional mitral regurgitation: implications for transcatheter mitral valve implantation. *Cardiovasc Ultrasound* 16: 27, 2018. doi:10.1186/s12947-018-0145-8.
9. **Mosteller RD.** Simplified calculation of body-surface area. *N Engl J Med* 317: 1098, 1987. doi:10.1056/NEJM198710223171717.
10. **Coisne A**, **Pontana F**, **Aghezzaf S**, **Mouton S**, **Ridon H**, **Richardson M**, **Polge AS**, **Longere B**, **Silvestri V**, **Pagniez J**, **Bical A**, **Rousse N**, **Overtchouk P**, **Granada JF**, **Hahn RT**, **Modine T**, **Montaigne D.** Utility of three-dimensional transesophageal echocardiography for mitral annular sizing in transcatheter mitral valve replacement procedures: a cardiac computed tomographic comparative study. *J Am Soc Echocardiogr* 33: 1245–1252.e2, 2020. doi:10.1016/j.echo.2020.04.030.
11. **van Wijngaarden SE**, **Kamperidis V**, **Regeer MV**, **Palmen M**, **Schalij MJ**, **Klautz RJ**, **Bax JJ**, **Ajmone Marsan N**, **Delgado V.** Three-dimensional assessment of mitral valve annulus dynamics and impact on quantification of mitral regurgitation. *Eur Heart J Cardiovasc Imaging* 19: 176–184, 2018. doi:10.1093/ehjci/jex001.
12. **Apor A**, **Nagy AI**, **Kovacs A**, **Manouras A**, **Andrassy P**, **Merkely B.** Three-dimensional dynamic morphology of the mitral valve in different forms of mitral valve prolapse – potential implications for annuloplasty ring selection. *Cardiovasc Ultrasound* 14: 32, 2015. doi:10.1186/s12947-016-0073-4.
13. **Badano LP**, **Caravita S**, **Rella V**, **Guida V**, **Parati G**, **Muraru D.** The added value of 3-dimensional echocardiography to understand the pathophysiology of functional tricuspid regurgitation. *JACC Cardiovasc Imaging* 14: 683–689, 2020. doi:10.1016/j.jcmg.2020.04.029.
14. **Lakatos BK**, **Kiss O**, **Tokodi M**, **Tősér Z**, **Sydó N**, **Merkely G**, **Babity M**, **Szilágyi M**, **Komócsin Z**, **Bognár C**, **Kovács A**, **Merkely B.** Exercise-induced shift in right ventricular contraction pattern: novel marker of athlete's heart? *Am J Physiol Heart Circ Physiol* 315: H1640–H1648, 2018. doi:10.1152/ajpheart.00304.2018.
15. **Kovacs A**, **Apor A**, **Nagy A**, **Vago H**, **Toth A**, **Nagy AI**, **Kovats T**, **Sax B**, **Szeplaki G**, **Becker D**, **Merkely B.** Left ventricular untwisting in athlete's heart: key role in early diastolic filling? *Int J Sports Med* 35: 259–264, 2013. doi:10.1055/s-0033-1349076.
16. **Hirasawa K**, **Izumo M**, **Umemoto T**, **Suzuki K**, **Kitanaka Y**, **Oi K**, **Mizuno T**, **Harada T**, **Ashikaga T**, **Miyairi T**, **Arai H**, **Hirao K**, **Akashi YJ.** Geometry of tricuspid valve apparatus in patients with mitral regurgitation due to fibroelastic deficiency versus Barlow disease: a real-time three-dimensional transesophageal echocardiography study. *J Am Soc Echocardiogr* 33: 1095–1105, 2020. doi:10.1016/j.echo.2020.04.019.
17. **Dal-Bianco JP**, **Aikawa E**, **Bischoff J**, **Guerrero JL**, **Handschumacher MD**, **Sullivan S**, **Johnson B**, **Titus JS**, **Iwamoto Y**, **Wylie-Sears J**, **Levine RA**, **Carpentier A.** Active adaptation of the tethered mitral valve: insights into a compensatory mechanism for functional mitral regurgitation. *Circulation* 120: 334–342, 2009. doi:10.1161/CIRCULATIONAHA.108.846782.
18. **Ruppert M**, **Lakatos BK**, **Braun S**, **Tokodi M**, **Karime C**, **Olah A**, **Sayour AA**, **Hizoh I**, **Barta BA**, **Merkely B**, **Kovacs A**, **Radovits T.** Longitudinal strain reflects ventriculoarterial coupling rather than mere contractility in rat models of hemodynamic overload-induced heart failure. *J Am Soc Echocardiogr* 33: 1264–1275.e4, 2020. doi:10.1016/j.echo.2020.05.017.
19. **Tokodi M**, **Németh E**, **Lakatos BK**, **Kispál E**, **Tősér Z**, **Staub L**, **Rácz K**, **Soltész Á**, **Szigeti S**, **Varga T**, **Gál J**, **Merkely B**, **Kovács A.** Right ventricular mechanical pattern in patients undergoing mitral valve surgery: a predictor of post-operative dysfunction? *ESC Heart Fail* 7: 1246–1256, 2020. doi:10.1002/ehf2.12682.
20. **Guta AC**, **Badano LP**, **Tomaselli M**, **Mihalcea D**, **Bartos D**, **Parati G**, **Muraru D.** The pathophysiological link between right atrial remodeling and functional tricuspid regurgitation in patients with atrial fibrillation. A three-dimensional echocardiography study. *J Am Soc Echocardiogr*, 2021 Jan 10 (online ahead of print). doi:10.1016/j.echo.2021.01.004.
21. **Muraru D**, **Addetia K**, **Guta AC**, **Ochoa-Jimenez RC**, **Genovese D**, **Veronesi F**, **Basso C**, **Iliceto S**, **Badano LP**, **Lang RM.** Right atrial volume is a major determinant of tricuspid annulus area in functional tricuspid regurgitation: a three-dimensional echocardiographic study. *Eur Heart J Cardiovasc Imaging*, 2020 Dec 2 (online ahead of print). doi:10.1093/ehjci/jeaa286.